Numerical simulation and experimental validation on hydrodynamic radial force of mixed-flow pump impeller

Ou Mingxiong[1], Shi Weidong[2], Jia Weidong[1], Fu Qiang[2]

(1. *Key Laboratory of Modern Agricultural Equipment and Technology, Ministry of Education, Jiangsu University, Zhenjiang* 212013, *China*; 2. *National Research Center of Pumps and Pumping System Engineering and Technology, Zhenjiang* 212013, *China*)

Abstract: This paper presents a numerical investigation of hydrodynamic radial force of mixed-flow pump, through validations and CFD simulations under several flow rates, the global performances of the mixed-flow pump is accurately predicted with RNG *k-ε* turbulence model, the head prediction error is less than 4.4% under all the operational conditions. The recirculation between the impeller and diffuser dominates the flow passage at part-load conditions, the pressure amplitude at 4 times shaft frequency was bigger than other frequencies, it increased sharply while the flow rate changed from 0.6 to 0.4 nominal flow rate, these demonstrated that the rotor-stator impeller blade passing excitation strengthened the pressure amplitudes of points between the impeller and diffuser under part-load conditions. The transient hydrodynamic radial forces of impeller present a periodicity change with time, the average value of transient radial force is close to zero under a uniform inflow condition. The FFT spectrum analysis of radial forces demonstrated that the amplitude of hydrodynamic radial forces under part-load conditions are much higher than nominal condition, especially at 1 time and 4 times shaft frequency, these phenomena are mainly attributed to the hydraulic imbalance of rotor, rotor-stator impeller blade passing excitation, rotor-stator blade interaction excitation and etc. Based on the analysis above, it is concluded that the recirculation flow pattern under part-load conditions has a significant influence on pressure fluctuation and hydrodynamic radial force.

Key words: pumps; impellers; spectrum analysis; hydrodynamic radial force; mixed-flow pump; rotor-stator interaction; recirculation; part-load condition

doi：10.11975/j.issn.1002−6819.2015.09.012

CLC number: TH313 **Document code:** A **Article ID:** 1002−6819(2015)−09−0071−06

Ou Mingxiong, Shi Weidong, Jia Weidong, et al. Numerical simulation and experimental validation on hydrodynamic radial force of mixed-flow pump impeller[J]. Transactions of the Chinese Society of Agricultural Engineering (Transactions of the CSAE), 2015, 31(9): 71－76. (in English with Chinese abstract)

欧鸣雄，施卫东，贾卫东，等. 斜流泵叶轮水力径向力的数值模拟与试验验证[J]. 农业工程学报，2015，31(9)：71－76.

0 Introduction

Mixed-flow pump is widely applied in many industrial and agricultural applications, such as sewage treatment, power plant, flood drainage and irrigation pump station[1]. The hydraulic model of mixed-flow pump is designed based upon the assumption that the flow in both the impeller and diffuser is steady and irrelevant, nevertheless, the rotor-stator interaction between impeller and diffuser can results in excitation forces under design flow-rate and an even stronger forces under off-design flow-rates[2-3], as the important component of excitation forces, the hydrodynamic radial forces impair the reliability of impeller, shaft and bearings[4-5].

The hydrodynamic forces applied on impeller are difficult to solved with theoretic method[6-7], Agostinelli et al. and Iversen et al. were the first to investigate the lateral excitation on an impeller in a vane-less volute[8-9]. The test facilities installed on shaft or bearing structure which used to measure steady hydrodynamic radial force, however, are hardly to access the precise values of hydrodynamic radial forces due to rotor-stator interaction[10-11]. In order to investigate the hydrodynamic forces of mixed-flow pump, Nyrenda designed a precise dynamometer which consist of 24 strain gauges, and measured the hydrodynamic radial forces of mixed-flow pump under non-uniform inlet velocity profiles[12]. Van Esch investigated the transient hydrodynamic radial forces of mixed-pump impeller through CFD (Computational Fluid Dynamics) simulation, the components of forces from CFD simulation model were agreed with experimental results approximately[13-14]. Cheng Li built a CFD model of mixed-flow water-jet pump, and the results show a good quantitative agreement with experimental data, this proved the validity of CFD model used in hydrodynamic radial forces prediction[15]. Kruger et al. did CFD analysis of vertical mixed-pump installed in a sump, the vortexes distribution in sump around pump inlet and hydrodynamic radial force applied on impeller were agreed with experiment results[16]. It is concluded that CFD

Received date: 2015-02-03 Revised date: 2015-04-17

Foundation item: National Natural Science Foundation of China (51475215, 51275215); Scientific Research Foundation of Jiangsu University (14JDG030); A Project Funded by the Priority Academic Program Development of Jiangsu Higher Education Institutions (PAPD).

Biography: Ou Mingxiong, Male, Hunan Province, Ph.D., Engaged in the research of numerical analysis and design of centrifugal pump. Zhenjiang, Key Laboratory of Modern Agricultural Equipment and Technology, Ministry of Education, Jiangsu University, 212013, China. Email: myomx@ujs.edu.cn.

simulation method is a valid mean for pump's transient hydrodynamic force prediction and analysis. This paper present a numerical investigation on hydrodynamic radial force of mixed-flow pump under several operational conditions, meanwhile, the flow field distribution and pressure fluctuation were investigated and explain how the flow pattern and rotor-stator interaction phenomena changed at part-load conditions, and finally, some meaningful conclusions were drawn.

1 Mixed-flow pump model

1.1 Design parameters

The parameters of the mixed-flow pump at the design operational condition as follow: nominal flow rate Q_0=1 450 m^3/h, nominal head H=12.5 m, rotational speed n=1 450 r/min, shaft frequency f_0=n/60=24.2 Hz, specific speed N_s=505, the diffuser and the elbow outlet pipe of the mixed-flow pump were designed as shown in Fig.1[17].

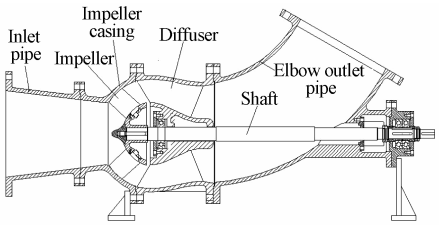

Fig.1 Cross section of test pump (without motor)

1.2 Test pump and parameters

The cross-section of the test pump is shown in Fig.1, the test pump assembly mainly includes impeller, shaft, inlet pipe, impeller casing, diffuser, elbow outlet pipe and et al. The main geometric parameters of the test pump were listed in Table 1.

Table 1 Main geometric parameters of test pump

Parameters	Values
Suction diameter D_i/mm	350
Discharge diameter D_o/mm	400
Inlet diameter d_1/mm	260
Outlet mean diameter d_2/mm	345
Blade wrap angle φ/(°)	84
Impeller blade number $z1$	4
Diffuser blade number $z2$	7

2 Numerical model and validation

2.1 Computational domain

The computational domain of the mixed-flow pump was generated according to the test pump's geometric dimensions, it consist of four sub-domains, namely inlet pipe, impeller, diffuser, elbow outlet pipe and out pipe, as shown in Fig.2. The lengths of outlet pipe and inlet pipe were extended to 3 times the pipe diameter, to increasing the simulation robustness[18]. In order to predict the global performance accurately, the clearance between blade tip and impeller casing was modeled in impeller sub-domain[19]. The whole computational domain geometry was modeled and assembled in Pro-E software.

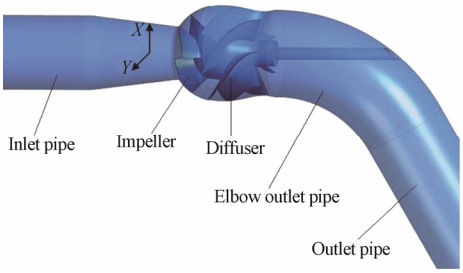

Fig.2 Sketch of computational domain

2.2 Boundary conditions

The inlet boundary condition was specified as a uniform inflow, the outlet boundary condition was assumed to outflow for fully developed flow. The turbulent flow in near-wall region was solved by standard wall function and all solid wall were set to be no-slip wall condition. The impeller sub-domain has a rotational movement, whereas the other sub-domains are in a stationary frame, the implicit multiple reference frames (MRF) method was adopted to resolve the governing equations of fluid flow in steady simulation, and sliding mesh model (SMM) method was adopted in unsteady simulation, the rotor-stator interaction between impeller and diffuser domain was simulated through non-Conformal interface algorithm[20].

2.3 Numerical method and setup

This study utilized the ANSYS FLUENT 14.0 commercial code to solve the Reynolds averaged Navier-Stokes (RANS) equations for the unsteady flow in the computational domain, according to the previous validation research in reference [13] and [15], RNG k-ε turbulence model was used to close the RANS equations in simulation, The flow in the impeller and diffuser was computed in a rotating frame of reference and a stationary frame of reference respectively, the SMM method supported in FLUENT was used to simulation the transient flow between the impeller and diffuser domain. The discretization of convection term and diffusion term used second order upwind scheme and central difference scheme respectively[21], the residuals convergence criterion was set to 0.0001. SIMPLE and PISO algorithm were selected to solve pressure-velocity coupling for steady and unsteady simulation respectively, the steady simulation was finished firstly as the initial solution for corresponding unsteady simulation which included changes in relative position between impeller and diffuser meshes. The time step size in unsteady simulation was 0.000345s, corresponding to an angular rotation of 3° for impeller[22]. After the periodical stable results were achieved in the unsteady simulations, There was one full impeller revolution results recorded for later analysis, the forces applied on impeller were monitored during every time step in unsteady simulations. There are six operational conditions from 0.2Q_0 to 1.2Q_0 were simulated, the results will be analyzed and compared with experimental results.

2.4 Grid generation

The grid generation process was carried out in ANSYS Workbench software, considering the whole computational domain consist of 5 sub-domains, the multi-block grid

method was used in grid generation. The hexahedral grids were generated in the inlet pipe and outlet pipe domains, the tetrahedral grids were generated in impeller, diffuser and elbow outlet pipe domains as shown in Fig.3. The clearance distance between blade tip and impeller casing is 0.2 mm, in order to take the leakage flow effect into account, the grids near the clearance were refined.

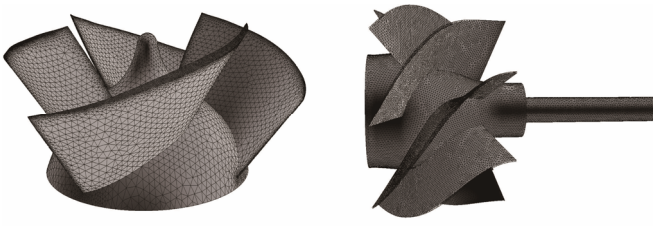

a. Impeller surface mesh　　b. Diffuser surface mesh

Fig.3　Grids of computational domain

The accuracy and error of CFD results are influenced by the number and quality of computational grids, through a grid sensitivity analysis based on steady simulation, the numerical results are independent from the number of grid nodes , the maximum non-dimensional wall distance y^+ of numerical model is less than 120, the details of grids are shown in Table 2.

Table 2　Grids statistics

Item	Value
Number of elements	2373817
Number of nodes	660128
Element quality	0.23
Skewness factor	0.73
Orthogonal quality	0.4

2.5　Global performance validation

The test pump's global performance data were obtained through a closed loop test system built according to grade 1 of national standard (GB 3216-2005), the systematic uncertainties of the test pump's head and power were less than 1%, the volumetric flow rate of the test pump was measured by a turbine flow-meter, the pressures at the inlet and outlet of the test pump were measured by pressure transmitter. The comparison of the experimental and numerical global performance curves is shown in Fig.4, the numerical global performance curves are consistent with experiment results under all operational conditions. The maximum head prediction error defined by Formula 1 is 4.4%[23], the differences between experimental and numerical results are mainly attributed to the geometric discrepancies, mechanical loss and uncertainty of the measurement. The pressures at the inlet and outlet of the test pump were measured by pressure transmitter, whereas the numerical determination of the pressure was achieved by an integration of the pressure distributions on the inlet and outlet pipe section, this is also an important factor influenced the results difference.

$$e=\frac{H_{\mathrm{Exp}}-H}{H_{\mathrm{Exp}}}\times 100\% \tag{1}$$

Where, e is the head prediction error, H_{Exp} is the experimental head of test pump, H is the head of numerical model.

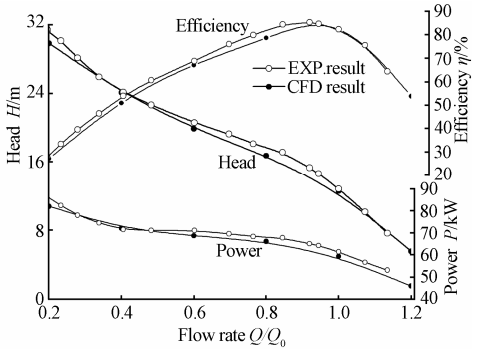

Fig.4　Comparison of global performances

3　Results and analysis

3.1　Flow distribution and pressure fluctuation

The forces acted on rotor are mainly determined by the flow field distribution of pump, the transient radial forces generated from the solid surfaces of impeller by time-dependent pressure distribution are influenced by the flow patterns[24]. The streamline distribution of meridian plane under different flow rates are presented in Fig.5, the recirculation between the impeller's trailing edge and the diffuser's leading edge can be observed obviously.

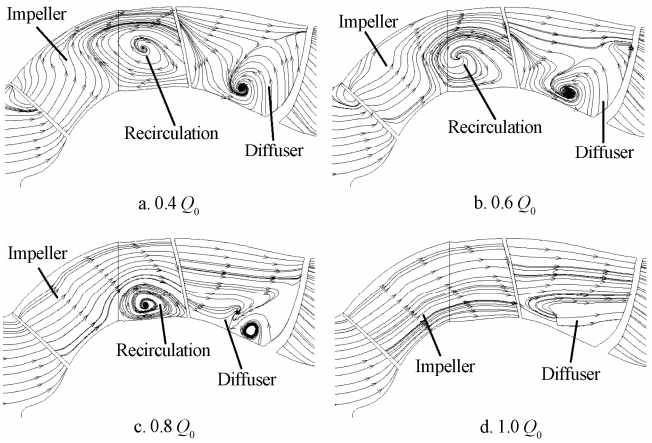

Fig.5　Streamline distribution chart in meridian plane

As shown in Fig.5, the recirculation at $0.4Q_0$ spread over the whole impeller-diffuser flow passage, it shrinks gradually with decreased flow rate, and disappeared at $1.0Q_0$. The recirculation dominates the flow passage at part-load conditions as a 3-dimensional dynamic vortex, in order to investigate the pressure fluctuation details result from rotor-stator interaction, the pressure amplitudes of points p1-p4 (as shown in Fig.6) under different flow rates were monitored and analyzed by Fast Fourier Transform (FFT) method, the spectrum analysis results of points p1-p4 were shown in Fig.7. The pressure amplitude at 4 times shaft frequency changed with flow rates as shown in Fig.8, it increased sharply while the flow rate changed from 0.6 Q_0 to 0.4 Q_0, and achieved its maximum value due to the strong rotor-stator impeller blade passing excitation.

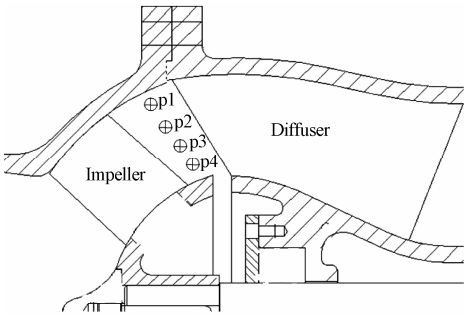

Fig.6 Pressure monitor points

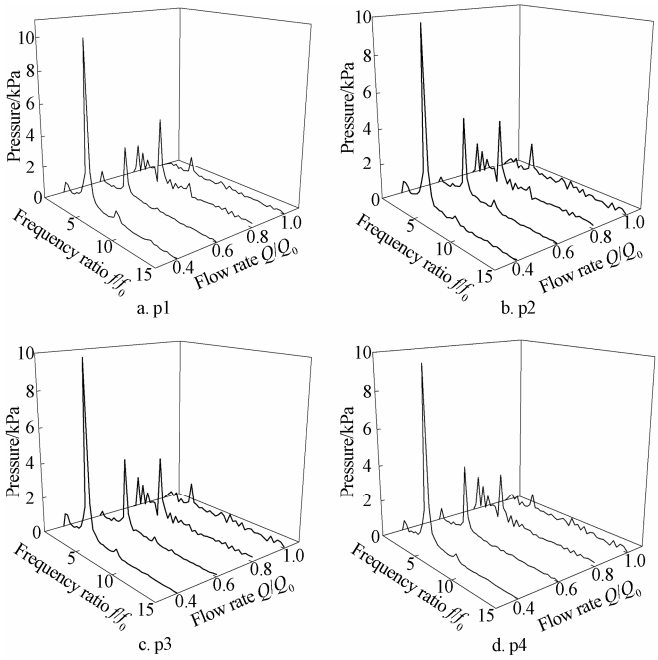

Fig.7 Spectrum analysis of points p1-p4

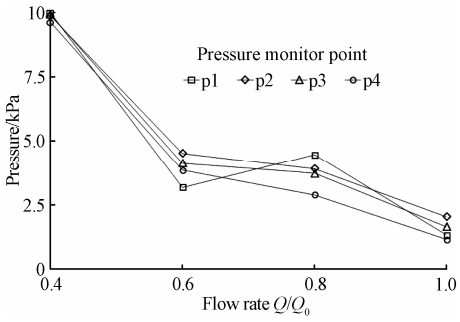

Fig.8 Pressure amplitude at 4 times shaft frequency

3.2 Hydrodynamic radial force in time domain

The direction and magnitude of transient hydrodynamic radial forces applied on impeller change with impeller rotation all the time, the transient dynamic forces data could be calculated through the unsteady CFD simulation. The components of transient hydrodynamic radial forces F_r along X and Y coordinates (shown in Fig.2) in every time step were shown in Fig.9, and the force vectors distribution in inertial frame of reference were shown in Fig.10.

The periodicity of transient hydrodynamic radial forces can be clearly observed in Fig.9, the steady components of transient hydrodynamic radial forces are close to zero, and the center points of force vector distribution are also close to original point of coordinate diagram obviously as shown in Fig.10. These phenomena validated the investigation of the hydrodynamic radial forces under non-uniform inflow condition stated in reference[14], and it is concluded that the steady hydrodynamic radial forces of impeller are mainly influenced by inflow profile.

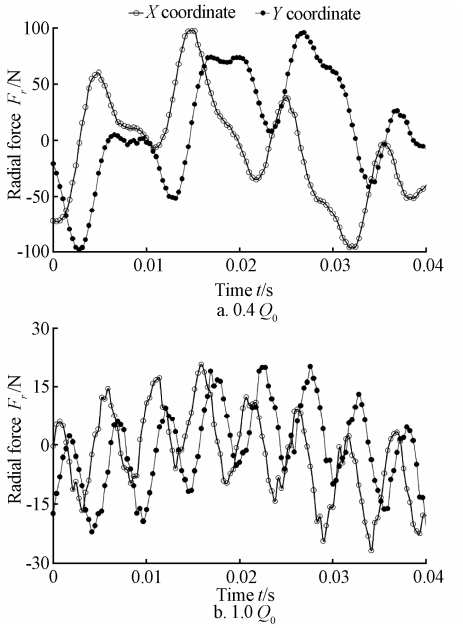

Fig.9 Hydrodynamic radial force curve in typical flow rate (over time)

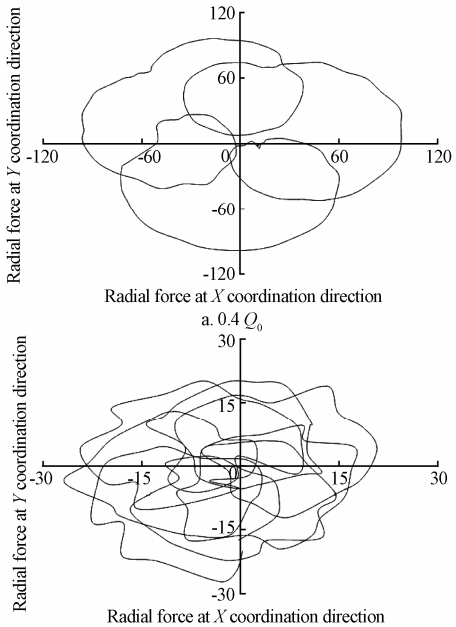

Fig.10 Hydrodynamic radial force vector distribution (one rotation)

The periodicity of transient hydrodynamic radial forces can be clearly observed in Fig.9, the steady components of transient hydrodynamic radial forces are close to zero, and the center points of force vector distribution are also close to original point of coordinate diagram obviously as shown in Fig.10. These phenomena validated the investigation of the hydrodynamic radial forces under non-uniform inflow

condition stated in reference[14], and it is concluded that the steady hydrodynamic radial forces of impeller are mainly influenced by inflow profile.

3.3 Hydrodynamic radial force in frequency domain

The Fast Fourier Transform (FFT) spectrum analysis of the transient hydrodynamic radial forces F_r under several operational conditions were shown in Fig.11, there are three peak values in chart of F_r (include at X coordination direction F_{rx} and at Y coordination direction F_{ry}) under 1 time, 4 times and 8 times shaft frequency. The peak values under different shaft frequency are mostly coursed by the hydraulic imbalance of rotor, rotor-stator impeller blade passing excitation, rotor-stator blade interaction excitation and etc[25].

The amplitude of hydrodynamic radial forces at 1 time, 4 times and 8 times shaft frequency under different operational conditions were shown in Fig.12. It is obviously observed that the amplitude of F_{rx} at 1 time shaft frequency increased from 2.9N to 49.2N, and the amplitude of F_{rx} at 4 times shaft frequency increased from 4.2N to 40.5N, meanwhile, the amplitude of F_{ry} at 1 time shaft frequency increased from 5.1N to 52.5N, and the amplitude of F_{ry} at 4 times shaft frequency increased from 3.3N to 40.9N, while the flow rate changed from 0.6 Q_0 to 0.4 Q_0. Though the amplitude of F_r at 8 times is less affected by operational conditions, it just increased from 11.7N to 16.2N in X coordinate direction and 11.6N to 15.4N in Y coordinate direction. These indicated that the transient hydrodynamic radial forces of the impeller become much bigger under part-load conditions, the results agree with the investigation reported in the reference[24].

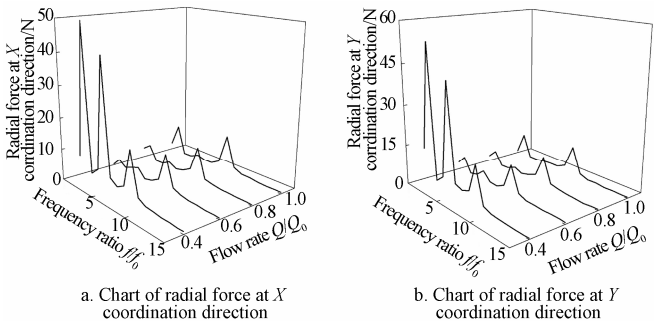

a. Chart of radial force at X coordination direction　　b. Chart of radial force at Y coordination direction

Fig.11　Spectrum analysis of hydrodynamic radial force

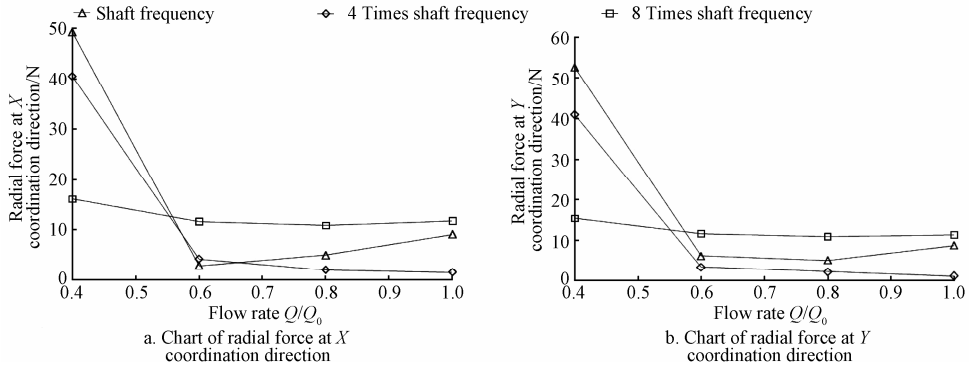

a. Chart of radial force at X coordination direction　　b. Chart of radial force at Y coordination direction

Fig.12　Radial force curves at different frequencies

4 Conclusions

1) The global performance of mixed-flow pump can be accurately predicted by CFD simulation based on appropriated setups, the maximum head prediction error is 4.4%, and the numerical results are in accordance with experimental results under all the operational conditions.

2) The recirculation between the impeller and diffuser dominates the whole flow passage at part-load conditions, meanwhile the pressure fluctuation analysis indicated that the rotor-stator impeller blade passing excitation strengthened the pressure amplitudes of points p1-p4 at part-load conditions.

3) The steady component of hydrodynamic radial force is decided by inflow condition under all the operational conditions, and the average value of transient radial force in one rotation time is close to zero. The FFT spectrum analysis demonstrated that the hydraulic imbalance of impeller and the rotor-stator impeller blade passing excitation influenced the hydrodynamic radial forces deeply under part-load conditions. Based on the analysis above, it is concluded that the recirculation flow patterns of mixed-flow pump under part-load conditions have a significant influence on pressure fluctuation and hydrodynamic radial force.

[References]

[1] Bing Hao, Cao Shuliang, Tan Lei, et al. Parameterization of velocity moment distribution and its effects on performance of mixed-flow pump[J]. Transactions of the Chinese Society of Agricultural Engineering (Transactions of the CSAE), 2012, 28(13): 100－105. (in Chinese with English abstract)

[2] Thomas A L. Reduction of Unsteady Rotor-stator Interaction Using Trailing Edge Blowing[D]. Blacksburg: Virginia Polytechnic Institute, 1997.

[3] Jacquet R G, Torkhani M. Rotor to stator contacts in turbomachines: Review and application[J]. Mechanical Systems and Signal Processing, 2013, 40(2): 401－420.

[4] Rodriguez C, Egusquiza E. Frequencies in the vibration induced by the rotor stator interaction in a centrifugal pump turbine[J]. Journal of Fluids Engineering, 2007, 129(11): 1428－1435.

[5] Zhang M, Tsukamoto H. Unsteady hydrodynamic forces due to rotor-stator interaction on a diffuser pump with identical number of vanes on the impeller and diffuser[J]. Journal of Fluids Engineering, 2005, 127(4): 743－751.

[6] Agostinelli A, Nobles D, Mockridge C R. An experimental investigation of radial thrust in centrifugal pumps[J]. J Eng Gas Turbines Power, 1960, 82(2): 120－125.

[7] Iversen H W, Rolling R E, Carlson J. Volute pressure distribution, radial force on the impeller, and volute mixing losses of a radial flow centrifugal pump[J]. Journal of Fluids Engineering, 1960, 82(2): 136－143.

[8] Yoshida Y, Tsujmoto Y, Ohashi H, et al. Rotordynamic forces on an open-type centrifugal compressor impeller in whirling motion[J]. ASME Journal of Fluids Engineering, 1999, 121(2): 259－265.

[9] Adkins D R, Brennen C E. Analyses of hydrodynamic radial forces on centrifugal pump impellers[J]. ASME Journal of Fluids Engineering, 1988, 110(1): 20－28.

[10] Guo S, Okamoto H, Maruta Y. Measurement on the fluid forces induced by rotor-stator interaction in a centrifugal pump[J]. JSME International Journal, Series B: Fluids and Thermal Engineering, 2006, 49(2): 434－442.

[11] Chamieh D S, Acosta A J, Brennen C E, et al. Experimental measurements of hydrodynamic radial forces and stiffness matrices for centrifugal pump[J]. ASME Journal of Fluids Engineering, 1985, 107(3): 307－315.

[12] Nyrenda P J. Experimental Study of Hydrodynamic Forces in Mixed-Flow Pump[D]. Eindhoven: Eindhoven University, 2004.

[13] Van Esch B P M. Numerical and experimental investigation of hydrodynamic forces due to non-uniform suction flow to a mixed-flow pump[C]. Proceedings of the ASME: Fluids Engineering Division Summer Meeting and Exhibition, 2005, Houston, USA, 2005: 1236－1242.

[14] Van Esch B P M. Performance and radial loading of a mixed-flow pump under non-uniform suction flow[J]. ASME Journal of Fluids Engineering, 2009, 131(5): 11－17.

[15] Cheng Li, Bart P M. Radial force of water-jet propulsion mixed-flow pump[J]. Journal of Drainage and Irrigation Machinery Engineering, 2012, 30(6): 636－640. (in Chinese with English abstract)

[16] Kruger S, Bouziad Y A, Maurer W. Pump sump CFD for vertical pump design[C]. Proceedings of the ASME: Fluids Engineering Division Summer Conference, 2009, Colorado, USA, 2009: 191－198.

[17] Ou Mingxiong. Research on Development and Flow-field Characteristic of Seawater Circulation Pump in AP1000 Nuclear Power Plant[D]. Zhenjiang: Jiangsu University, 2013. (in Chinese with English abstract).

[18] Shi Weidong, Zhou Ling. Numerical prediction and performance experiment in a deep-well centrifugal pump with different impeller outlet width[J]. Chinese Journal of Mechanical Engineering, 2013, 26(1): 46－52.

[19] Shi Weidong. Performance prediction and circulation distribution analysis at impeller inlet and outlet of mixed-flow pump[J]. Transactions of Chinese Society for Agricultural Machinery, 2011, 42(9): 94－97. (in Chinese with English abstract)

[20] Li Deyou, Wang Hongjie. Unsteady simulation and analysis for hump characteristics of a pump turbine model[J]. Renewable Energy, 2015, 77: 32－42.

[21] Barrio R, Fernandez J, Blanco E, et al. Estimation of radial load in centrifugal pumps using computational fluid dynamics[J]. European Journal of Mechanics B/Fluids, 2011, 30(3): 316－324.

[22] Zhang Desheng. Unsteady flow analysis and experimental investigation of axial-flow pump[J]. Journal of Hydrodynamics, 2010, 22(1): 35－43.

[23] Felix A M, Peter H, Philippe D. CFD calculation of a mixed flow pump characteristic from shutoff to maximum flow[J]. ASME Journal of Fluids Engineering, 2002, 124(11): 798－802.

[24] Pei J, Dohmen H. Investigation of unsteady flow-induced impeller oscillations of a single-blade pump under off-design conditions[J]. Journal of Fluids and Structures, 2012, 35: 89－104.

[25] Christopher E Brennen. Hydrodynamics of Pumps[M]. Cambridge: Cambridge University Press, 2011.

斜流泵叶轮水力径向力的数值模拟与试验验证

欧鸣雄[1]，施卫东[2]，贾卫东[1]，付　强[2]

（1. 江苏大学现代农业装备与技术教育部重点实验室，镇江 212013；
2. 国家水泵及系统工程技术研究中心，镇江 212013）

摘　要：该文采用数值分析法研究了斜流泵叶轮的水力径向力变化规律，通过数值模拟准确地预测了斜流泵的水力性能，扬程预测误差在 4.4%以内。通过数值分析获得了斜流泵叶轮的瞬态水力径向力数据，均匀进口条件下，叶轮的瞬态水力径向力均值几乎为零。对瞬态水力径向力进行傅里叶分析，获得其在频域内的分布，结果显示，当工况从 0.6 倍设计流量点变至 0.4 倍设计流量点时，1 倍和 4 倍轴频下的径向力突然增大，叶轮的水力不平衡和动静干涉中的叶片通过激励增强了上述频率下的水力径向力数值。流场分析显示，在小流量工况时，叶轮与导叶体之间的回流涡旋完全占据了泵内流道空间。进一步的压力脉动分析证实，在小流量工况下，动静干涉中的叶片通过激励显著增大了叶轮与导叶之间测试点的压力脉动幅值。

关键词：泵；叶轮；光谱分析；水力径向力；斜流泵；动静干涉；回流涡旋；小流量工况